Showcasing research from the *In Situ* Ion Irradiation Transmission Electron Microscopy (I^3TEM) Facility within the Ion Beam Laboratory at Sandia National Laboratories.

In situ TEM ion irradiation and implantation effects on Au nanoparticle morphologies

Real time nanoscale observation of ion beam modification of gold nanoparticles, and sequential electron tomography revealing 3-D information about the induced structural changes.

As featured in:

See Khalid Hattar *et al.*, *Chem. Commun.*, 2014, **50**, 7593.

ROYAL SOCIETY OF CHEMISTRY

www.rsc.org/chemcomm

Registered charity number: 207890

ChemComm

COMMUNICATION

View Article Online
View Journal | View Issue

Cite this: *Chem. Commun.*, 2014, **50**, 7593

Received 13th December 2013,
Accepted 19th February 2014

DOI: 10.1039/c3cc49479a

www.rsc.org/chemcomm

In situ TEM ion irradiation and implantation effects on Au nanoparticle morphologies†

Daniel Bufford,[a] Sarah H. Pratt,[a] Timothy J. Boyle[b] and Khalid Hattar*[a]

Energetic heavy and light ion effects on gold nanoparticles were probed by irradiating 20 and 60 nm diameter nanoparticles with either 3 MeV Cu^{3+} or 10 keV He^{+} ions *in situ* inside of a transmission electron microscope. Both ion species caused sintering, agglomeration, and ablation of the nanoparticles *via* sputtering, although at different rates.

Nanomaterials promise unique physical and chemical properties in comparison to bulk material properties primarily due to their increased surface-area-to-volume ratios.[1] Therefore, a wide range of diverse fields are investigating the utility of nanoparticles (NPs), including some in harsh radiation environments.[2] Subtle changes to the size, shape, surface chemistry, and internal structure of NPs have been found to strongly influence their final properties (*e.g.*, functionality and toxicity).[1,3] Without fundamentally understanding radiation-induced alterations to a NP's structure, any resulting property changes cannot be reliably predicted. This lack of understanding may limit the utility of NPs in proposed efforts like extra-atmospheric solar cells,[2] clinical radiation therapies,[4] or as signal enhancers in secondary ion mass spectrometry.[5]

Some irradiation effects on NPs have been proffered, such as the studies detailing shape modification of NPs embedded in a matrix like SiO_2 for potential plasmonic device applications,[6] but these studies were limited to bound NPs. Irradiation effects in "unbound" NPs have received significantly less study due to both the difficulty of performing such experiments and, until recently, a perceived lack of utility for the results of such studies.[6] Recent studies with relatively light and low energy ions have manipulated the photoluminescence of quantum dots[6] and the magnetic properties of FePt NPs.[6] Investigations of NPs irradiated by heavier ions with increasing energies up to the GeV range[6–10] have demonstrated a range of effects depending on the collision dynamics including: ejection of increasingly large clusters, up to 10^5 atoms per ion,[10] and ion channelling with minimal sputtering.[9] Many of these studies were computational and would benefit from experimental validation.

In situ transmission electron microscopy (TEM) experiments can address length and time scales intermediate between those reported by molecular dynamics (MD) simulations[6–9] and *ex situ* experiments.[6,10] Recent *in situ* irradiation TEM experiments have revealed an order of magnitude or more increase in the sputter yields of Au nanorods, due to both size-induced enhancement of typical sputtering processes, and processes unique to nanomaterials, like "explosive ejection" of large clusters.[11] This limited set of reported *in situ* irradiation TEM experiments on NPs leaves a wide range of NP sizes, shapes, and compositions, in addition to ion species, energies, dose rates, and total doses to explore.

The *in situ* ion irradiation TEM (I^3TEM) facility within the Ion Beam Laboratory at Sandia National Laboratories allows observation of specimens *in situ* during ion bombardment. The I^3TEM is unique in that it allows for concurrent high- and low-energy ion beams of a broad range of species through the same port, minimising potential directional effects like shadowing. In order to compare effects of a broad range of ion energies and masses on Au NPs, two drastically different irradiation conditions were chosen: (i) low dose rate, energetic, heavy ions (3 MeV Cu^{3+}), and (ii) high dose rate, lower energy, light ions (10 keV He^{+}). These experiments were designed to provide initial insight into ion species-, energy-, and dose-rate dependent processes that affect the morphology of unbound NPs during ion beam irradiation.

In the first part of this study, Au NPs were deposited by drop casting from an aqueous suspension of citrate-stabilised Au NPs (concentration $\sim 7.2 \times 10^{11}$ particles per mL) onto holey carbon TEM grids. The specimens were irradiated with 3 MeV Cu^{3+} ions at a flux of $\sim 7.5 \times 10^{11}$ Cu^{3+} per cm^2 per s. The NPs were imaged at 15 min intervals ($\sim 0.75 \times 10^{15}$ Cu^{3+} per cm^2) until a total irradiation time of 4 h ($\sim 1.1 \times 10^{16}$ Cu^{3+} per cm^2) was reached. The NPs measured in Fig. 1 were not under continuous observation during irradiation, which minimised any electron beam effects (see ESI†). As received, Au NPs were nominally uniform and 20 ± 2.4 nm in diameter. Sintering and limited internal structure change occurred up to

[a] *Sandia National Laboratories, PO Box 5800-1056, Albuquerque, NM 87185, USA. E-mail: khattar@sandia.gov; Tel: +1 505 845-9859*
[b] *Sandia National Laboratories, Advanced Materials Laboratory, 1001 University Boulevard SE, Albuquerque, NM 87106, USA*

† Electronic supplementary information (ESI) available. See DOI: 10.1039/c3cc49479a

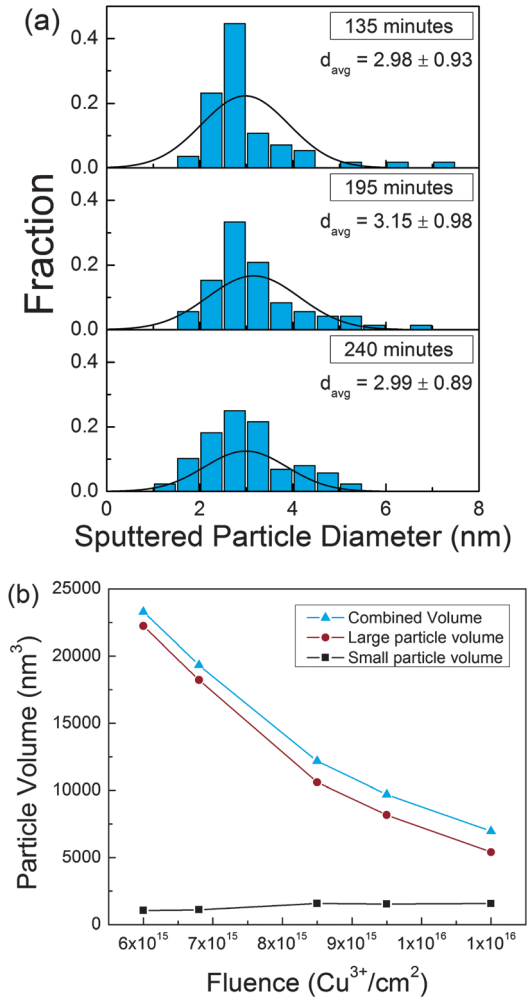

Fig. 1 (a) Histograms showing the size distribution of sputtered particles from micrographs (Fig. S2d–f, ESI†). (b) Plot showing total particle volume as a function of time, revealing substantial volume loss. Error bars are smaller than the symbols.

75 min (~3.4 × 10^{15} Cu^{3+} per cm^2) (Fig. S2a and b, ESI†). The morphology changed significantly by 90 min (~4.1 × 10^{15} Cu^{3+} per cm^2); the NPs had coalesced into a single mass, twin and grain boundaries were not distinguishable, and a surrounding halo of ejected material had formed (Fig. S2c, ESI†). Smaller particles in the halo of material continued to increase in number at the expense of the coalesced mass. From 135 to 240 min (~6–11 × 10^{15} Cu^{3+} per nm^2), the large agglomerated particle decreased from 17 to 11 nm in diameter, while average sputtered particle diameter remained nearly constant at ~3 nm (Fig. 1a).

NP volume was estimated from the particle projected area measured from micrographs (see ESI†). While the sputtered particle volume increased slightly during this time, the total particle volume decreased by ~70% (Fig. 1b). Clearly identifiable sputtered particles like those in Fig. S2d–i (ESI†) only appeared within a few tens of nm from the parent particle cluster. Hence, sputtered material may be either (1) spread finely over a large area and not agglomerated to a degree possible to observe using bright-field TEM imaging or (2) not captured on the carbon grid (*i.e.*, dispersed into the column).

In order to obtain information on the 3-D shape and location of the initial NPs and sputtered material, 3-dimensional tomograms were collected. After collecting an initial tomography tilt series on one group of Au NPs, the sample was irradiated with 3 MeV Cu^{3+} at a flux of ~8.5 × 10^{11} Cu^{3+} per cm^2 per s for 30 min (fluence of ~1.6 × 10^{15} Cu^{3+} per cm^2). Two more tomography tilt series of the same region were similarly collected to yield 3 tilt series over a total fluence ~3.1 × 10^{15} Cu^{3+} per cm^2 of *in situ* ion irradiation. The NPs in Fig. 2 were continuously observed during ion irradiation, and likely show increased sintering due to the electron beam.[12] However, it appears that the ion irradiation effects dominated, as the overall structural changes appear similar to those seen in the previous section. Furthermore, these changes were far more drastic than sintering induced by the electron beam alone (see ESI†).

The 3-D models (Fig. 2 and ESI† movies) revealed the resulting 3-D NP shape and location of sputtered material. For example, rotation of the tomogram in Fig. 2d revealed a previously unobserved particle (indicated by the arrow) that was obscured in Fig. 2c. Tomograms also revealed tiny NPs present on the back side of the carbon support film (Fig. 2f). It is not clear whether these small NPs resulted from migration from the original, sputtering through the carbon film, or sputtering from other NPs outside the field of view.

Since Cu^{3+} ions at 3 MeV have a predicted average penetration depth in solid Au of ~650 nm,[13] very few ions were expected to stop within the NPs (see ESI†). It is believed that the small size of the NPs enhances the sputtering yield compared to the bulk,[8,11] as sputtering is sensitive to the amount of energy deposited near the surface by the damage cascade. In addition, energetic ions may induce cascades too large to be contained within many of the NPs, resulting in ejections of up to thousands of atoms during particularly violent collisions.[9,11] It is reasonable to assume that some collisions may have ejected Au atoms on the order of hundreds of nm. Similarly enhanced sputtering has been seen previously in embedded NP studies.[6]

There is also the question of localised thermal effects. Thermal energy from incident ions may diffuse readily in thermally connected material, but would be confined within an isolated NP. Heating a 20 nm Au NP from room temperature to its melting point (1064 °C), then melting it requires ~1.55 × 10^{-14} J or 97 × 10^3 eV at most (see ESI†). An upper-bound for the energy deposited by a single ion can be estimated by considering a head-on collision, where energy transfer is given by: $T_m = 4M_1M_2E_0/(M_1 + M_2)^2$. Here, M_1 and M_2 are the atomic masses of the ion and atom species, and E_0 is the incident ion energy.[14] For 3 MeV Cu^{3+} ions colliding with Au the maximum is ~73%, or 2.2 MeV, more than 20 times the energy needed to melt the entire particle. Even without direct knock-on, an ion can deposit significant energy *via* electron interactions. For 3 MeV Cu^{3+} ions in Au, this electronic stopping is an estimated 2.7 keV nm^{-1}.[13] Therefore, even for a 10 nm path with no nuclear interactions, a Cu^{3+} ion would deposit ~27 keV, which is enough energy to increase the temperature of a 20 nm NP by over 400 °C.

The energy deposited during both nuclear and electronic interactions with Cu ions is certainly enough to induce considerable changes to NP size and morphology. Changes in structure, such as the loss of internal twin boundaries, noted in Fig. S2a (ESI†), and rounding of the initially faceted NPs (*e.g.*, Fig. S2a–c, ESI†) were interpreted as possible signs that enough energy was deposited in the

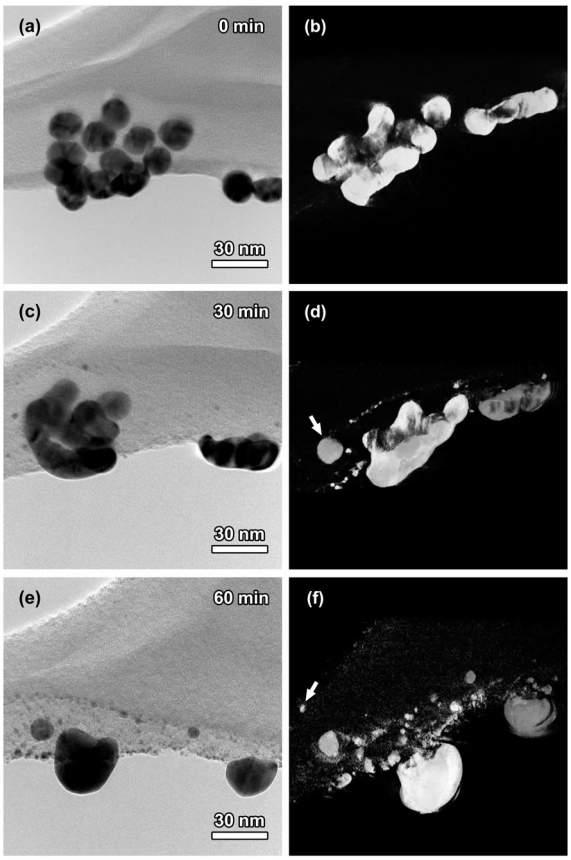

Fig. 2 Source electron micrographs and discrete 4-D electron tomograms of Au NPs irradiated with 3 MeV Cu^{3+}. (a, c, e) Example micrographs from tilt series collected after [min (exposure $\times$ 10^{15} Cu^{3+} per cm^2)]: (a) 0, (b) 30 ($\sim$1.6), (c) 60 ($\sim$3.1). (b, d, f) Corresponding 3-D tomogram reconstructions, rotated to a different angle from the source micrograph (see ESI† for more images).

NPs to induce transient internal amorphisation.[15] Coalescence of Au NPs and subsequent sputtering-induced shrinking of the large mass in Fig. 1 and 2 suggest an inverse Ostwald ripening process.[16] Interestingly, overall sputtered particle size changed little; the most notable occurrence was that larger (>6 nm) particles disappeared. Eventually, agglomeration and sputtering rates may result in a stable equilibrium NP size. The data in Fig. 1a may hint at a stable size, but the nearby large particle likely acted as a local source of new material. Further work with more controlled sources of material to sputter is needed to determine the validity of this hypothesis.

The combined data from conventional micrographs and tomograms indicate that Cu^{3+} bombardment produced significant changes within the NPs, beginning with removal of internal grain boundaries, to agglomeration and shape change, to the formation of finer ejected NPs. These processes were accompanied by substantial volume loss over time, and ejected material was dispersed over the front and back sides of the carbon grid.

In an effort to explore a lower mass and energy system than Cu^{3+}, a subsequent implantation study was performed using 10 keV He^+ ions. The ion irradiation was performed with the TEM electron beam blanked, and images were collected quickly to minimise electron beam effects. The flux was $\sim 1 \times 10^{15}$ He^+ per cm^2 per s, and the sample was irradiated up to 90 min (total fluence $\sim 1.3 \times 10^{18}$ He^+ per cm^2). The NPs used here were $\sim$60 nm in diameter (see ESI† for synthesis information), and included some plate-like structures (Fig. 3a). Images were collected at 2, 5, 10, 20, 45, and 90 min. For this sample, after 2 min ($\sim 1.3 \times 10^{17}$ He^+ per cm^2) of irradiation the onset of sintering was apparent, and after 10 min ($\sim 6.6 \times 10^{17}$ He^+ per cm^2) the formation of dislocation loops and the onset of sputtering (Fig. 3c) were apparent. Both sintering and sputtering increased until the experiment was stopped at 90 min ($\sim 5.9 \times 10^{18}$ He^+ per cm^2, Fig. 3e).

Several oddities were noted during these He^+ implantation experiments. First, nearby ($\sim$100 nm) sputtered material halos often appeared inhomogeneous and, in some cases, were absent from certain particles and regions. It is not immediately apparent whether this was an effect from material emission or particle coalescence mechanics. The sputtering process itself might have directional dependencies due to channelling or ion incidence direction, or emitted material distributions may be affected by shadowing or overlapping sputtered material halos. It is also possible that local features of the carbon grids may affect nucleation and growth of the sputtered material. Second, NPs under continuous observation during irradiation showed less ejected material than those not continuously under the electron beam. There is the possibility that the

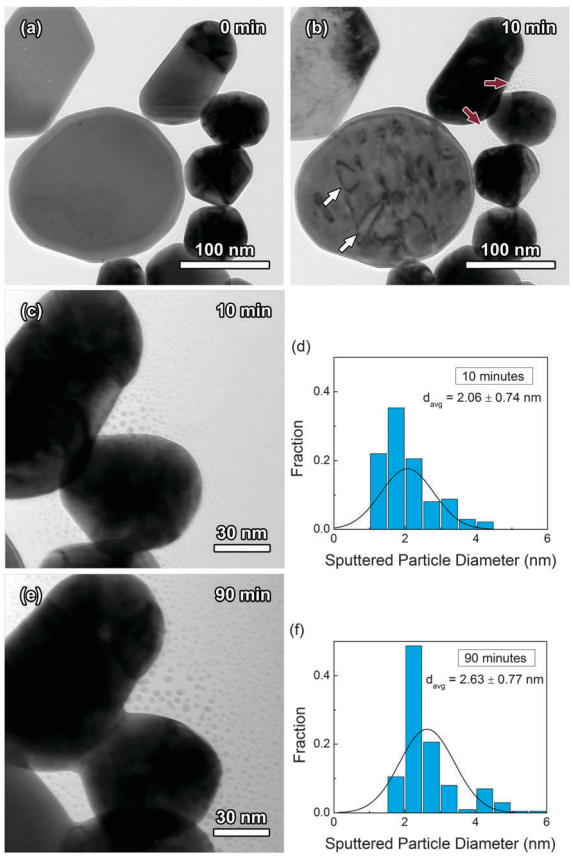

Fig. 3 Micrographs showing (a) initial Au NPs structure and during *in situ* ion irradiation with 10 keV He^+ after (b–d) 10 min ($\sim 6.6 \times 10^{17}$ He^+ per cm^2), and (e and f) 90 min ($\sim 5.9 \times 10^{18}$ He^+ per cm^2). In (b) red and white arrows indicate sputtered material and dislocation loops, respectively.

electron beam may have influenced sputtering behaviour, or the diffusion and agglomeration behaviour of the sputtered material.

While the He^+ sputtered material appeared qualitatively similar to that of the Cu^{3+} case, several key differences between the Cu^{3+} and He^+ irradiation cases should be discussed. First, TRIM (Transport of Ions in Matter[13]) simulations (see ESI†) estimated that 10 keV He^+ ions should have an average range of ~36 nm in thick solid Au. Inspection of the simulated ion trajectories in the Au layer revealed a great number of internally recoiled and scattered ions, resulting in a broad location distribution of implanted He atoms. Hence, when simulating a thinner 20 nm layer, most He^+ ions escaped, and only ~2% of the incident ions stopped within the Au layer. Accordingly, no He bubbles were observed in this study, despite the very low solubility of He in Au.[17]

Second, due to the disparity in the atomic masses of He and Au, the maximum energy transfer is ~7.8%, or 780 eV. Since 10 keV He^+ ions produce far smaller cascades than those from 3 MeV Cu^{3+} ions, consequences of such cascades (cluster emission, transient amorphisation) are likely absent. Still, 780 eV is still quite large in comparison to individual bond energy, so collisions with near-surface Au atoms would be expected to cause sputtering. Electronic stopping power is only 0.093 keV nm^{-1}, nearly 300 times less than in the Cu^{3+} case. Therefore, the electronic heating of a 20 nm NP due to a single ion is expected to be on the order of 1 °C.

Third, nominal power density, taken as the ion flux times ion energy, was not drastically different: ~0.4 W cm^{-2} for Cu^{3+} and ~1.6 W cm^{-2} for He^+, although the kinetics involved in energy delivery were quite different. The amount of energy dissipated into the layer may be roughly estimated by using TRIM simulations (see ESI†). On an average per-ion basis, Cu^{3+} deposited more than 20 times the energy of He^+ ions; however, due to the difference in flux, for a given time interval the Cu^{3+} deposited only about 0.03 times the energy of He^+. Given the fluxes reported earlier and a spherical 20 nm particle with projected area = πr^2, ~2.5 collisions per s are expected from Cu^{3+} ions, compared to over 3100 collisions per s for He^+. Surprisingly, even with such differences in energy delivery, both ion species induced substantial sputtering. Independent of the irradiation conditions employed, the energy delivered each second was more than enough to melt the particle but only in the Cu^{3+} case did significant internal structure changes occur. Additional experiments will be necessary to determine the roles of ion mass, energy, flux, and mounting in sputtering and thermal energy dissipation during bombardment.

Many questions remain regarding the physics and chemistry of ion interactions with nanomaterials. In addition to a physical and chemical understanding of radiation tolerance in NPs, this work provides exploratory insight into ion beam modification that may potentially be employed to alter nanomaterials, or to form nanostructures not currently possible by other means. For example, Cu^{3+} bombardment caused significant internal structure change, while both ion species induced surface structure changes and sintering. Also, the sputtering and agglomeration processes observed in this work indicated that ~2–3 nm diameter NPs may be made from larger NPs by He^+ implantation or Cu^{3+} bombardment. The new smaller NPs or other far-from-equilibrium nanostructures produced by ion beam modification may have new unstudied properties of interest.

In conclusion, the I^3TEM facility allowed for *in situ* ion irradiation studies of the radiation stability of unbound Au NPs under various irradiation conditions. This initial study elucidated the structural damage caused to nearly freestanding Au NPs, as a function of dose in the extreme radiation conditions of 3 MeV Cu^{3+} (~1.1×10^{16} ions per cm^2) and 10 keV He^+ (~1.3×10^{18} ions per cm^2). During Cu^{3+} irradiation, Au NPs coalesced into one mass, then underwent extreme volume loss as material was sputtered away, resulting in a multitude of sputtered particles ranging from 1 to 5 nm in diameter. Ablation and rapid sputtering was explained by inverse Ostwald ripening and the large NP surface-area-to-volume ratio arguments, respectively. In addition, electron tomography coupled with *in situ* ion irradiation resulted in a series of 3D models of the structural damage highlighting the volume evolution of the NPs. Irradiation with 10 keV He^+ produced sintering and dislocation loop formation by ~1.3×10^{17} He^+ per cm^2, followed by noticeable sputtering by ~6.6×10^{17} He^+ per cm^2, and continuing to up to a fluence of ~1.3×10^{18} He^+ per cm^2. Resulting coalesced particles ranged from ~1.5 to 5.5 nm in diameter. This exploratory study demonstrates the radiation tolerance of Au NPs, as a function of irradiation conditions.

The authors thank K. Jungjohann, B. A. Hernadez-Sanchez, A. N. Kinghorn, J. S. Custer, and D. L. Buller (Sandia National Laboratories) for their helpful assistance and discussions. This work was supported by the Division of Materials Science and Engineering, Office of Basic Energy Sciences, U.S. Department of Energy. Sandia National Laboratories is a multi-program laboratory managed and operated by Sandia Corporation, a wholly owned subsidiary of Lockheed Martin Corporation, for the U.S. Department of Energy's National Nuclear Security Administration under contract DE-AC04-94AL85000.

Notes and references

1 M. C. Daniel and D. Astruc, *Chem. Rev.*, 2004, **104**, 293–346.
2 M. G. Lines, *J. Alloys Compd.*, 2008, **449**, 242–245.
3 M. Ferrari, *Nat. Rev. Cancer*, 2005, **5**, 161–171.
4 E. Porcel, S. Liehn, H. Remita, N. Usami, K. Kobayashi, Y. Furusawa, C. Le Sech and S. Lacombe, *Nanotechnology*, 2010, **21**, 085103.
5 A. Marcus and N. Winograd, *Anal. Chem.*, 2006, **78**, 141–148.
6 A. V. Krasheninnikov and K. Nordlund, *J. Appl. Phys.*, 2010, **107**, 071301.
7 R. Kissel and H. M. Urbassek, *Int. J. Mass Spectrom.*, 2001, **208**, 29–35.
8 T. T. Jarvi and K. Nordlund, *Nucl. Instrum. Methods Phys. Res., Sect. B*, 2012, **272**, 66–69.
9 S. Zimmermann and H. M. Urbassek, *Int. J. Mass Spectrom.*, 2008, **272**, 91–97.
10 I. Baranov, S. Kirillov, A. Novikov, V. Obnorskii, M. Toulemonde, K. Wien, S. Yarmiychuk, V. A. Borodin and A. E. Volkov, *Nucl. Instrum. Methods Phys. Res., Sect. B*, 2005, **230**, 495–501.
11 G. Greaves, J. A. Hinks, P. Busby, N. J. Mellors, A. Ilinov, A. Kuronen, K. Nordlund and S. E. Donnelly, *Phys. Rev. Lett.*, 2013, **111**, 065504.
12 Y. Chen, R. E. Palmer and J. P. Wilcoxon, *Langmuir*, 2006, **22**, 2851–2855.
13 J. F. Ziegler, M. D. Ziegler and J. P. Biersack, *Nucl. Instrum. Methods Phys. Res., Sect. B*, 2010, **268**, 1818–1823.
14 M. A. Nastasi, J. W. Mayer and J. K. Hirvonen, *Ion-solid interactions: fundamentals and applications*, Cambridge University Press, Cambridge, New York, 1996.
15 T. T. Jarvi, A. Kuronen, K. Nordlund and K. Albe, *J. Appl. Phys.*, 2007, **102**, 124304.
16 G. C. Rizza, M. Strobel, K. H. Heinig and H. Bernas, *Nucl. Instrum. Methods Phys. Res., Sect. B*, 2001, **178**, 78–83.
17 J. Laakmann, P. Jung and W. Uelhoff, *Acta Metall. Mater.*, 1987, **35**, 2063–2069.

